

Formation of nitric acid/water ice particles in cirrus clouds

B. Kärcher¹ and C. Voigt¹

Received 5 February 2006; revised 1 March 2006; accepted 21 March 2006; published 26 April 2006.

[1] Nitric acid (HNO₃) in cirrus ice crystals has been measured in the last decade during airborne field campaigns at latitudes 53°S–68°N. The HNO₃ content in ice crystals, expressed in terms of HNO₃/H₂O molar ratio, and the fraction of HNO₃ in ice derived from those measurements exhibit a clear upward trend with decreasing temperature. The observations are explained by a novel model describing dissolution of HNO₃ in liquid aerosol particles serving as freezing nuclei and subsequent trapping of HNO₃ during ice crystal growth. The efficiency of trapping increases with decreasing temperature. Efficient trapping occurs via diffusional burial of the ambient HNO₃ below about 203 K, because of long residence times of HNO₃ molecules at the ice surface. This opens the possibility for HNO₃-induced modifications of processes affecting ice crystal growth. At warmer temperatures, molecular processes in the ice surface layer cause an increasingly rapid escape of adsorbed HNO₃ into the gas phase and render trapping less efficient despite faster ice growth rates. **Citation:** Kärcher, B., and C. Voigt (2006), Formation of nitric acid/water ice particles in cirrus clouds, *Geophys. Res. Lett.*, *33*, L08806, doi:10.1029/2006GL025927.

1. Introduction

[2] The study of nitric acid (HNO₃) uptake in cirrus cloud particles is an important focus in airborne field campaigns (SUCCESS [Weinheimer *et al.*, 1998], POLSTAR [Schlager *et al.*, 1999], SOLVE [Kondo *et al.*, 2003], INCA [Ziereis *et al.*, 2004], CRYSTAL/FACE [Popp *et al.*, 2004], EUPLEX [Voigt *et al.*, 2006]), spanning tropical to polar latitudes. These measurements cover anvil clouds associated with subtropical deep convection, midlatitude stratiform cirrus and wave clouds, and Arctic cirrus. The studies revealed significant reductions of gas phase HNO₃ in the presence of ice at low temperatures and high HNO₃ partial pressures, but a consistent and physically plausible theoretical explanation is lacking.

[3] We argue that the frequently applied concept of an instantaneous adsorption equilibrium is not adequate to describe the formation of mixed HNO₃/H₂O particles in cirrus clouds. Ice crystals are hardly found in equilibrium with H₂O in the gas phase, and consequently, the HNO₃ content in individual crystals results from an integration of HNO₃ uptake and evaporation over their entire life cycles. Hence, the amount of HNO₃ taken up by cirrus particles cannot simply be correlated to instantaneous variables like cloud surface area density, but is determined by variability

in ice supersaturation and ice crystal fall speeds, and the spatial distribution of HNO₃.

[4] To this end, we developed a model of trace gas uptake in growing ice crystals (trapping) which combines surface kinetic and gas diffusion processes of, e.g., HNO₃ along with condensing H₂O vapor [Kärcher and Basko, 2004]. A recent laboratory study of enhanced HNO₃ uptake in ice films growing in a flow tube generally supports this trapping concept [Ullerstam and Abbatt, 2005], but it remains unclear whether such results are applicable to real atmospheric conditions. On the other hand, individual cirrus measurements are difficult to compare with cloud model results because of the nonlocal character of the uptake process. Here we use an approach that integrates many measurements covering a very wide range of cirrus cloud properties.

[5] We demonstrate that two limiting cases of trapping – namely (partial) retention of HNO₃ molecules contained in freezing aerosol particles followed by (i) pure dilution by subsequent deposition of H₂O on ice or (ii) further uptake of all available ambient HNO₃ during ice crystal growth – bound the body of observed molar HNO₃/H₂O ratios in cirrus. An approximate expression for the efficiency of trapping derived on the basis of the field measurements is capable of describing the observed temperature trends of average molar ratios and ice phase fractions of HNO₃ and allows us to delineate important atmospheric implications.

2. Trapping Model

[6] The molar HNO₃/H₂O ratio per cirrus ice particle is given by

$$\mu = \frac{\omega N_n + \Delta N_n}{N_w + \Delta N_w}, \quad (1)$$

where N_n and N_w are equilibrium numbers of HNO₃ and H₂O molecules in the aerosol particles when freezing commences, and ΔN_n and ΔN_w are the numbers of molecules taken up during subsequent ice particle growth. We assume the homogeneously freezing aerosol to be composed of supercooled ternary (H₂O/HNO₃/H₂SO₄) solution (STS) particles. The parameter ω accounts for three mechanisms that may alter N_n . The aerosol composition may not be at equilibrium because of diffusion-limited uptake rates of HNO₃; only a fraction of the HNO₃ molecules may be locked in the ice particles after freezing (retention effect); and the aerosol particles may not be pure STS particles but could contain, e.g., ammonium or solid inclusions.

[7] Next we define the molar HNO₃/H₂O ratio per freezing particle:

$$\mu_a = \omega \frac{N_n}{N_w} = \omega \frac{m_w}{m_n} \frac{W_n}{W_w}. \quad (2)$$

¹Institut für Physik der Atmosphäre, Deutsches Zentrum für Luft- und Raumfahrt, Oberpfaffenhofen, Germany.

The last expression follows from $N_j = \rho V W_j / m_j$ ($j = n, w$), with the molecular masses m_j and the volume V , mass density ρ , and equilibrium species mass fractions W_j of the aerosol particles. The steady-state molar HNO₃/H₂O ratio in ice particles is defined by

$$\mu_\infty = \frac{\Delta N_n}{\Delta N_w} = \frac{D_n}{D_w} \frac{p_n}{e_i s_i} \frac{\epsilon}{\beta_w}. \quad (3)$$

The last expression in (3) follows from the ratio of diffusional vapor fluxes dN_j/dt as given by the trapping model [Kärcher and Basko, 2004, equation (11)]. Here, D_j are gas diffusion coefficients, p_n is the ambient HNO₃ partial pressure, e_i [mb] = 0.01 exp(28.868 – 6132.9/T [K]) is the ice saturation vapor pressure [Marti and Mauersberger, 1993], s_i is the net ice supersaturation the cirrus particles experience during their lifetime and which determines the average ice water content of a developed cloud, $\beta_j < 1$ are size-dependent flux corrections accounting for gas kinetic effects at high Knudsen numbers, and $0 \leq \epsilon \leq \beta_n$ is the trapping efficiency for HNO₃ defined in section 3.

[8] With these definitions (1) takes the convenient form

$$\mu = \mu_a \frac{1}{1 + \mathcal{N}} + \mu_\infty \frac{\mathcal{N}}{1 + \mathcal{N}}, \quad \mathcal{N} = \frac{\Delta N_w}{N_w}, \quad (4)$$

with $\Delta N_w = \rho_i (V_i - V) / m_w$ and the ice particle mass density ρ_i and volume $V_i \geq V$. The ice crystal volume neglects the contributions of HNO₃ and H₂SO₄ as they are small compared to H₂O. Because crystals sediment and likely fall through regions with different p_n , we do not consider the conservation of total HNO₃ in (4). Right after freezing, $\mathcal{N} = 0$ and we obtain the initial value $\mu = \mu_a$. We note two asymptotic cases for large ice particles, $\mathcal{N} \gg 1$: (i) $\mu \rightarrow \mu_\infty$ for $\epsilon > 0$ and (ii) $\mu \rightarrow \mu_a / \mathcal{N}$ for $\epsilon = 0$. Case (i) includes trapping of HNO₃ at maximum efficiency ($\epsilon = \beta_n$) and case (ii) assumes no HNO₃ uptake in the growing ice particles, i.e., pure dilution by uptake of H₂O.

[9] We note that trapping does not necessarily imply that buried HNO₃ is distributed over the entire ice particle volume. Instead, trapped molecules could stay within a small volume concentrated near the surface in case they are partially excluded from the crystal lattice during growth. Atmospheric HNO₃ concentrations are often too low to establish a monolayer coverage on the crystal surfaces.

[10] With the help of the ice water content, IWC, we introduce the partitioning factor ϕ as the ratio of the concentration of HNO₃ in ice, $\mu \text{IWC} / m_w$, to the total (gas plus ice phase) HNO₃ concentration. The total amount does not contain an aerosol contribution; although cloud-resolving simulations suggest that uptake of HNO₃ in STS particles can be substantial at high ice supersaturations prior to and shortly after homogeneous freezing, however, once enough ice crystals form and grow to average sizes, HNO₃ is redistributed between aerosol and ice particles and uptake in ice takes over [Kärcher, 2005]. Below we will connect IWC to s_i via $\text{IWC} = m_w n_i s_i$, with $n_i = e_i / (kT)$ (k is Boltzmann's constant), resulting in

$$\phi = \left(1 + \frac{p_n}{\mu e_i s_i}\right)^{-1} \xrightarrow{\mu \rightarrow \mu_\infty} \left(1 + \frac{D_w \beta_w}{D_n \epsilon}\right)^{-1}. \quad (5)$$

[11] We fix the ambient pressure p to 200 mb and use $\omega = 0.4$. The model results are not sensitive to p and the assumed total aerosol H₂SO₄ content $q_s = 0.1$ ppbv and freezing particle radius $r = 0.5 \mu\text{m}$ ($V = 4\pi r^3/3$). At equilibrium, STS particles of this size freeze homogeneously at approximate ice supersaturations $s^* = 1.35 - T$ [K]/259 [Koop *et al.*, 2000], which set the H₂O vapor mixing ratios $q_w = (1 + s^*)e_i/p$ used to determine W_j and ρ in the STS particles along with q_s and p_n [Kärcher and Solomon, 1999, section 2.2]. The values μ_a strongly decrease with increasing T . To evaluate β_j , we use the mass accommodation coefficients $\alpha_n = 0.3$ for HNO₃ and 0.5 for H₂O [Kärcher, 2005].

[12] The volume of an ice crystal is $V_i = 3\sqrt{3}D^2L/8$, $L = D/\mathcal{A}$ being the length of a hexagonal column, D its average base circumscribed diameter, and \mathcal{A} its aspect ratio. In the T -range 195–240 K, we suggest fits to a climatology of lidar and radar data [Wang and Sassen, 2002, Table 1] of average D and IWC for developed cirrus ($\mathcal{N} \gg 1$) of the form D [μm] = 1.2 T [K] – 221.6, with $\mathcal{A} = 0.8$ in this D -range, and IWC [mg/m^3] = exp(T [K]/15 – 13.33). These fits compare well to the original data within their error bounds; they improve the data below ~ 210 K, because most optically thin clouds remain undetected by the remote sensing leading to a sample bias in the retrievals. The mean D and IWC values are broadly consistent with *in-situ* measurements. The IWC defines $s_i = \text{IWC}/(m_w n_i)$; s_i increases from 0.06 (240 K) to 0.86 (195 K), which is reasonable as supersaturation relaxation times also increase [e.g., Kärcher, 2005].

[13] In what follows, we assume an average p_n together with the average T -dependencies of s_i and V_i to calculate the asymptotic cases of (4). We use an analytic expression for $\epsilon(T)$ in order to constrain the full solution (4) with the field measurements. This approach cannot track the histories of individual crystals, but provides a basic understanding of the main trends seen in the field data.

3. Results and Discussion

[14] Figure 1 (bottom) depicts $\mu(T, \bar{p}_n)$ from (4) (curves) along with T -averaged *in-situ* data (symbols) taken during the airborne measurements mentioned in section 1. We have used a constant value $\bar{p}_n = 2 \times 10^{-8}$ mb close to the average over all campaigns to calculate the asymptotic μ -values at maximum trapping, $\mu = \mu_\infty$ with $\epsilon = \beta_n$ (upper dashed curve), and those without trapping, $\mu = \mu_a / \mathcal{N}$ (lower dashed curve). Taken together, the HNO₃/H₂O ratios in ice and the corresponding fractions of HNO₃ in ice displayed in the top panel show a clear upward trend with decreasing T .

[15] We should be cautious not to overinterpret the data in Figure 1. All instruments (except the one employed during CRYSTAL/FACE) detect total reactive nitrogen and assume a fraction of it (20–80%) to be HNO₃ in the gas phase. The anisokinetic airborne sampling of particles leads to pressure- and size-dependent corrections to the actual ice phase HNO₃ concentrations which are associated with some uncertainty. The accuracy of IWC measurements used to derive μ depends in part on the presence of very large and very small ice crystals. Flight patterns are also relevant. Measurements taken in forming or dissolving clouds would lead to higher-than-average μ -values. Above

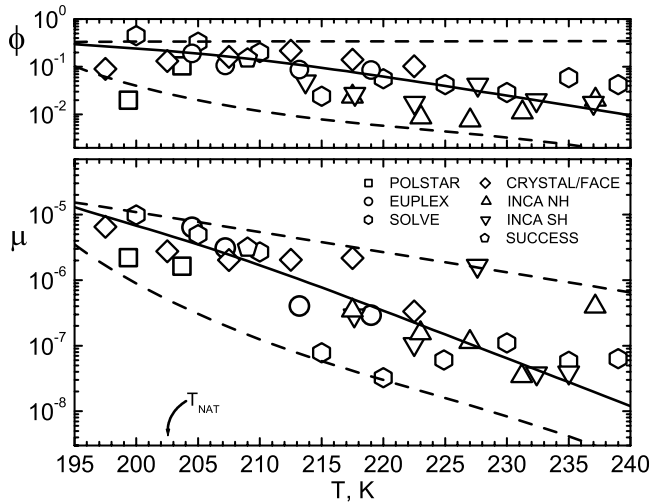


Figure 1. Molar $\text{HNO}_3/\text{H}_2\text{O}$ ratio μ and partitioning fraction ϕ of HNO_3 in cirrus ice as a function of temperature T . Except for POLSTAR and SUCCESS, the symbols represent 5 K-averages (mean values) of *in-situ* data taken during the airborne campaigns noted in the legend. (bottom) The solid curve is a fit to the μ -data using (4) and (6), and the dashed curves depict approximate lower (μ_a/\mathcal{N} with $\omega = 0.4$) and upper (μ_∞ with $\epsilon = \beta_n$) limits of trapping. (top) The ϕ -curves are computed from the corresponding μ -curves using (5). The variability of individual data points is significantly higher than measurement standard deviations which are typically comparable to the data point values. The curved arrow marks the average NAT existence temperature.

235 K, cirrus ice may form by homogeneous freezing of water droplets nucleated above water saturation. In super-cooled water droplets, HNO_3 is highly soluble, possibly leading to a higher HNO_3 content in ice after droplet freezing as compared to freezing of STS particles. This potential bias toward high μ is not captured by our uptake model.

[16] That being said, we very successfully bound the average behavior of the large body of field data (dashed curves) using the typical assumptions entering (4). Individual data points (averaged over 10 s, not shown but discussed in the original references) exhibit a large range of variability of uptake by about a factor of 10 above and below the mean μ -values shown in Figure 1. This scatter in μ is mainly caused by variations in p_n , factors determining IWC, and meteorological conditions prevailing during the measurements. Similar arguments hold for the ice partitioning coefficient ϕ .

[17] Reasons why we are not able to capture the full range of individual data variability in μ are easily explained. Individual data points can lie above the upper limit curve $\mu_\infty \propto p_n$. This may happen when p_n is larger than the average value \bar{p}_n used here. Also, ice particles can trap more than \bar{p}_n if they grow and fall long enough. Individual measurements can also lie below the lower limit curve $\mu_a/\mathcal{N} \propto \omega V/V_i$. Fewer HNO_3 molecules may be retained upon freezing and HNO_3 uptake may be limited by gas diffusion, which would reduce ω . A non-STs aerosol composition may enhance uptake, e.g., due to the presence of ammonium; on the other hand, solid inclusions such as dust reduce the liquid particle volume V and may initiate freezing below s^* ,

leading to less uptake. Another choice of V_i would also affect the lower limit. Fortunately, the overall trend of the mean μ -data is not strongly affected by the lower limit result (see below).

[18] The HNO_3 fractions in ice are more difficult to compare with our model results than the molar ratios. While the p_n -dependence of μ should be controlled by the abundance of HNO_3 present during ice growth, ϕ inferred from observations are computed based on local p_n -values. As ice crystals sediment, they might move into regions with different p_n than were present during their main growth phase. Presumably, this leads to many cases where measured partitioning factors do not represent true cloud averages and a comparison with model results loses relevance.

[19] To establish a parameterization, we note the trapping efficiency from Kärcher and Basko [2004], combining their equations (11) and (17), along with our empirical fit for $\xi(T)$ based on the field data:

$$\epsilon = \frac{\beta_n}{1 + (1 - \beta_n)\xi}, \quad \xi = \exp\left(33.5 - \frac{6345}{T[\text{K}]}\right). \quad (6)$$

The parameter $\xi = v_n/\dot{r}_i$ is defined as the ratio of the effective speed v_n with which adsorbed HNO_3 molecules leave the ice particle surface (and are not buried in the bulk ice) relative to the diffusional ice particle growth rate \dot{r}_i . The assumed functional form of ξ is meaningful because \dot{r}_i and likely v_n exhibit an Arrhenius-type T -dependence. An expression for v_n follows from ξ with $\dot{r}_i = m_w D_w \beta_w C n_s / (\rho_i \dot{r}_i)$, with the radius r_i of an ice crystal volume-equivalent sphere and the capacitance factor C . A ventilation correction can be ignored in this growth law as it is close to unity in our case.

[20] The desired mean molar ratio (bottom solid curve in Figure 1) is obtained by inserting (6) into (4) and fitting $\xi(T)$. From 195 to 240 K, \dot{r}_i increases from 0.3 to 2 $\mu\text{m}/\text{min}$ and ϵ decreases from 0.56 to 0.016. This ϵ -range corresponds to uptake coefficients $\gamma = \alpha_n/(1 + \xi) = 0.083 - 2.6 \times 10^{-4}$ [Kärcher and Basko, 2004, equation (13)]. The mean ice partitioning factors (top panel) are obtained from (5). At first glance, one might expect ϕ to rise with T because of increasing average IWC. However, as T rises, μ decreases at a faster pace than IWC increases. The combined effect results in the negative correlation between ϕ and T (solid curve), consistent with the main trend seen in the field measurements.

[21] Although the aerosol decay term $\mu_a/(1 + \mathcal{N})$ is not always smaller than the trapping term $\mu_\infty \mathcal{N}/(1 + \mathcal{N})$ in the full solution (4), especially at low T where ice crystals remain relatively small, we have checked that $\mu \approx \mu_\infty$ is a good approximation in the given range of T . Hence, for practical applications, it is sufficient to use (3) and (6) together with (5), eliminating the need to deal with assumed aerosol composition and retention factor that enter (4) via (2).

[22] For $p_n > 10^{-7}$ mb [Popp *et al.*, 2004], surface saturation effects may limit the amount of HNO_3 buried upon adsorption (by introducing a negative correlation of ϵ with p_n) and hence weaken the linear p_n -dependence of μ_∞ . However, such high p_n -values occur rarely and contribute only little to the entire data set. Nevertheless, the dependence of uptake on p_n should be studied in future extensions of the present work.

[23] In the trapping model, ξ determines the parameter combination $\beta_{n\kappa}\lambda = (1 - \beta_n)\xi$ [Kärcher and Basko, 2004, section 2.5] which separates two distinct trapping regimes. Our $\xi(T)$ from (6) leads to $\beta_{n\kappa}\lambda < 1$ below 203 K, defining a regime where HNO₃ molecules stay relatively long at the surface and diffusional burial controls the uptake. Above 203 K, $\beta_{n\kappa}\lambda > 1$; molecular processes that occur in the ice surface layer cause increasingly rapid escape of HNO₃ back into the gas phase (relative to the mean ice growth rate), rendering trapping less efficient.

[24] The fact that HNO₃ molecules stay relatively long at ice surfaces below 203 K is very interesting, as it paves the way for HNO₃-induced modifications of the H₂O deposition and ice growth kinetics below the nitric acid trihydrate (NAT) existence temperature T_{NAT} . For our average conditions $p_w = (1 + s_i)e_i$ and $p_n = \bar{p}_n$, we find $T_{\text{NAT}} = 202.6$ K; local T_{NAT} -values may differ by $\pm(1-2)$ K. Long residence times of HNO₃ in this regime might favor a transition to stable NAT clusters at the ice surface which subsequently interfere with active growth sites for H₂O molecules.

[25] Among all data taken in developed clouds shown in Figure 1, only the CRYSTAL/FACE data points in the 202.5 K- and 197.5 K-bins could possibly be influenced by the presence of NAT. (Measurements below $T_{\text{NAT}} + 2$ K are not included in the SOLVE data set [Kondo *et al.*, 2003].) While NAT-induced modifications of ice crystal growth at low T are apparent in concomitant observations of ice supersaturation [Gao *et al.*, 2004], such an effect is not visible in terms of μ and cannot be ascribed with certainty to the ϕ -data point at 197.5 K.

4. Summary and Conclusions

[26] Our discussion revealed the complexity of factors controlling observed molar HNO₃/H₂O ratios in cirrus ice and HNO₃ ice partitioning coefficients, but also showed that the available field measurements of uptake of HNO₃ in cirrus clouds can be integrated with the physical theory of trapping in growing ice crystals. Fitting an analytical expression for the trapping efficiency to the field data allowed us to constrain the model without the need to know the details of the molecular processes that occur at the ice particle surfaces. A key finding is that as the temperature decreases, trapping increases in importance.

[27] We offered a number of reasons causing the scatter of data points around our model results, among which are the large variability of controlling factors (e.g., ice water content, HNO₃ abundance) and the comparison of local measurements with model results based on a nonlocal process. At this stage of intercomparison between theory and observations, we see no practical way of significantly improving the data analysis. Despite the difficulty of tracking air parcel and ice crystal trajectories, we suggest targeted cloud sampling in future airborne campaigns. Together with cloud-resolving models employing Lagrangian ice particle tracking, this will allow more detailed comparisons to be performed.

[28] An increased residence time of HNO₃ molecules at the ice crystal surfaces at temperatures below the NAT

existence temperature, as suggested by our analysis, is a necessary prerequisite for efficient impurity pinning of surface growth steps, as proposed by Gao *et al.* [2004] to explain observations of enhanced relative humidity in cold subtropical anvil cirrus. This issue deserves more attention in the future.

[29] Our results are not directly comparable to the laboratory study of Ullerstam and Abbatt [2005], because these experiments used ice films possibly distinct from cirrus ice crystals, among other factors. It would be helpful to understand in which circumstances results of such important laboratory measurements can be applied to real atmospheric situations. An alternative is to carry out uptake experiments in cloud chambers with freely suspended ice particles such as reported by Diehl *et al.* [1995], but at temperatures below 235 K.

[30] **Acknowledgments.** We are grateful to H. Irie, Y. Kondo, P. Popp, H. Schlager, A. Weinheimer, and H. Ziereis for their support and acknowledge fruitful discussions with D. Fahey, J. Hendricks, M. Krämer, and D. Murphy. This study was funded by the European Commission in the SCOUT-O3 project.

References

- Diehl, K., S. K. Mitra, and H. R. Pruppacher (1995), A laboratory study of the uptake of HNO₃ and HCl vapor by snow crystals and ice spheres at temperatures between 0 and -40°C , *Atmos. Environ.*, **29**, 975–981.
- Gao, R. S., *et al.* (2004), Evidence that ambient nitric acid increases relative humidity in low-temperature cirrus clouds, *Science*, **303**, 516–520.
- Kärcher, B. (2005), Supersaturation, dehydration, and denitrification in Arctic cirrus, *Atmos. Chem. Phys.*, **5**, 1757–1772.
- Kärcher, B., and M. M. Basko (2004), Trapping of trace gases in growing ice crystals, *J. Geophys. Res.*, **109**, D22204, doi:10.1029/2004JD005254.
- Kärcher, B., and S. Solomon (1999), On the composition and optical extinction of particles in the tropopause region, *J. Geophys. Res.*, **104**, 27,441–27,459.
- Kondo, Y., *et al.* (2003), Uptake of reactive nitrogen on cirrus cloud particles in the upper troposphere and lowermost stratosphere, *Geophys. Res. Lett.*, **30**(4), 1154, doi:10.1029/2002GL016539.
- Koop, T., B. P. Luo, A. Tsias, and T. Peter (2000), Water activity as the determinant for homogeneous ice nucleation in aqueous solutions, *Nature*, **406**, 611–614.
- Marti, J., and K. Mauersberger (1993), A survey and new measurements of ice vapor pressure at temperatures between 170 and 250 K, *Geophys. Res. Lett.*, **20**, 363–366.
- Popp, P. J., *et al.* (2004), Nitric acid uptake on subtropical cirrus cloud particles, *J. Geophys. Res.*, **109**, D06302, doi:10.1029/2003JD004255.
- Schlager, H., *et al.* (1999), In-situ observations of particulate NO_y in cirrus clouds for different atmospheric conditions, in *Proceedings of the European Workshop on Aviation, Aerosols, Contrails, and Cirrus Clouds, Seeheim, Germany*, edited by U. Schumann and G. T. Amanatidis, pp. 68–73, Eur. Comm., Brussels.
- Ullerstam, M., and J. P. D. Abbatt (2005), Burial of gas phase HNO₃ by growing ice surfaces under tropospheric conditions, *Phys. Chem. Chem. Phys.*, **7**, 3596–3600.
- Voigt, C., *et al.* (2006), Nitric acid in cirrus clouds, *Geophys. Res. Lett.*, **33**, L05803, doi:10.1029/2005GL025159.
- Wang, Z., and K. Sassen (2002), Cirrus cloud microphysical property retrieval using lidar and radar measurements. Part II: Midlatitude cirrus microphysical and radiative properties, *J. Atmos. Sci.*, **59**, 2291–2302.
- Weinheimer, A. J., *et al.* (1998), Uptake of NO_y on wave-cloud ice particles, *Geophys. Res. Lett.*, **25**, 1725–1728.
- Ziereis, H., *et al.* (2004), Uptake of reactive nitrogen on cirrus cloud particles during INCA, *Geophys. Res. Lett.*, **31**, L05115, doi:10.1029/2003GL018794.

B. Kärcher and C. Voigt, Institut für Physik der Atmosphäre, Deutsches Zentrum für Luft- und Raumfahrt, Oberpfaffenhofen, D-82234 Wessling, Germany. (bernd.karcher@dlr.de)